JOURNAL OF CATALYSIS **178,** 253–263 (1998)
ARTICLE NO. CA982099

Tracking Down the Reduction Behavior of Copper-on-Alumina Catalysts

M. Fernández-García,*[,1] I. Rodríguez-Ramos,* P. Ferreira-Aparicio,* and A. Guerrero-Ruiz†

*Instituto de Catálisis y Petroleoquímica, CSIC, Campus Cantoblanco, 28049-Madrid, Spain; and †Departamento de Química Inorgánica, UNED, Senda del Rey, 28040-Madrid, Spain

Received January 27, 1998; revised April 6, 1998; accepted April 7, 1998

The evolution of copper-based catalysts during a reduction treatment has been followed using X-ray absorption near edge structure (XANES) in conjunction with a statistical analysis. Using this novel approach, we will provide evidence of (a) the number and nature of the active copper phases formed during the genesis of the catalysts, (b) their dependence on the chemical conditions of the preparation procedure, (c) the degree of reactivity of these phases toward hydrogen, and (d) details on the mechanism of the solid phase transformations during interaction with this molecule. Transmission electron microscopy (TEM) is used to complement results concerning the nature and physical properties (i.e. particle size) of copper phases, and in order to stress the importance of the XANES findings, conventional temperature programmed reduction (TPR) experiments are compared with a simulation of the hydrogen consumption occurred in the reduction process using the XANES results. © 1998 Academic Press

INTRODUCTION

Real time, real condition in situ techniques are analytical tools particularly resourceful in the area of heterogeneous catalysis (1–3). In the vast majority of cases, active phases are minority components in catalyst formulations so many techniques lack the sensitivity to detect or properly analyze these phases. Additionally, active phases exhibit only short or local range order with poorly resolved three-dimensional structures (4), a fact which hinders an extensive use of many conventional techniques, such as X-ray diffraction (XRD) for solid state characterization. Broadly speaking, the knowledge of the chemical (phase) behavior of a catalytic solid under the influence of a reactive environment is a point of vital importance for the understanding and prediction of its catalytic properties (5), the ultimate goal in the field of catalysis.

Here, we will show that this type of information may be obtained by performing a XANES study of copper-on-alumina catalysts. This system has been the subject of many investigations since the earliest days of spectroscopic characterization of catalysts (6) due to the apparent simplicity of the system and its variety of industrial applications (7), among which a potential recent addition could be the treatment of exhaust gas from nonstationary sources (8). In this system, several copper solid phases are possible: CuO and $CuAl_2O_4$ in oxidic environments, and Cu_2O, $CuAlO_2$, and Cu^0 in reductive atmospheres. The coexistence of these phases under some reduction conditions has induced numerous multitechnique approaches to the problem (9–11) which, however, have not been able to fully resolve a number of fundamental questions. Although reduction processes ascribed to CuO and $CuAl_2O_4$ have been distinguished (11), it is rather difficult to unequivocally state whether some Cu^{2+} ions are reduced directly to Cu^0 or if Cu^+ can be stabilized under specific experimental conditions. Cu^{2+} in aluminate matrixes also involves the additional complication of exhibiting varying fractional occupancies with the superficial/bulk characteristic of the copper phase for the two possible symmetry locations, octahedral and tetrahedral (9–11). Finally, certain physical (e.g. particle size) and chemical (e.g. oxygen vacancies or the interaction with the support) properties are likely to modify the thermal behavior of copper phases upon reduction (12, 13). The combination of these three effects eventually leads to results open to various interpretations to describe the reduction behavior of copper-on-alumina catalysts.

In aiming to alleviate the uncertainties related with these questions, we will perform a statistical analysis of XANES spectra taken during the reduction process of two copper-on-alumina catalysts. XANES results about the initial, oxidized state of the samples will be complemented with TEM data and the information concerning the reduction process compared with that obtained from conventional TPR experiments. To a good approximation, the temperature insensitivity of the electronic transitions (in vibronic coupling absence) means that the XANES technique is a suitable tool to study reduction or more generally catalytic processes. Additionally, the inherent atomic specificity of absorption techniques and the characteristic good signal-to-noise ratio of XANES makes it an optimum choice to allow a successful study of a solid minority component. The bulk

[1] Corresponding author. E-mail: ICPMF03@PINAR1.CSIC.ES.

0021-9517/98 $25.00

averaged absorption XANES signal recorded throughout a reduction treatment can yield a variety of information depending on the type of analysis performed; binding energy shift based or white line intensity based XANES can give some indication concerning the average oxidation state of the active element (14, 15), whereas a more quantitative treatment using the present statistical approach may fully capture the phase behavior of the system (16). On the other hand, it must be mentioned that this last, new approach has a notable advantage with respect to fitting procedures (as least squares minimization) as the number of free parameters, the number of copper species in our case, is rigorously chosen. Moreover, the expected intensity differences in the continuum resonances (induced by the different particle sizes) between a reference compound and supported particles may bring enough uncertainty to a fit involving more than two species to strongly limit its usefulness. Note, however, that the shape of a XANES spectra is dominated by the local symmetry and the position of the continuum resonances (CR) by the coordination distances and these parameters are preserved in a (much) larger extent that the intensity of the CRs, allowing the unequivocal assignation of copper species present in catalysts by comparison with reference materials (8, 16–19). Theoretical studies of the dependence of these variables with the particle size can be found in Refs. (18, 19).

EXPERIMENTAL AND COMPUTATIONAL DETAILS

Two CuO/Al_2O_3 samples were prepared and studied under temperature-programmed reduction (TPR) conditions. In the first, copper was impregnated onto γ-alumina (Puralox, Condea, $S_{BET} = 176\ m^2 \cdot g^{-1}$) support by adsorption of Cu^{2+} from a nitrate solution at ambient temperature while maintaining the pH at 9 using a $NH_4^+/NH_4^+OH^-$ buffer. The second was prepared by incipient wetness impregnation using an aqueous solution of $Cu(NO_3)_2$ ($pH \approx 1.9$). These samples are referred to as 3% Cu/Al_2O_3(OH) and 5% Cu/Al_2O_3(H), respectively, this nomenclature indicating the copper content as determined by atomic absorption analysis and the pH medium at which samples were prepared. Both samples were dried in air at 383 K and calcined for 2 h at 923 K. As will be shown, copper loadings were chosen in such a way that common copper phases have similar particle size distributions.

XANES experiments at the Cu K-edge were carried out in the ID-24 line at the ESRF Synchrotron, Grenoble. All samples, catalysts and pure reference compounds, were measured in an energy-dispersive, transmission mode with simultaneous calibration of the energy scale with the help of a Cu foil. A bent perfect Si crystal in a Bragg configuration was used as a dispersive monochromator. Self-supporting wafers of the samples were placed in a controlled-atmosphere (10% H_2 in He) cell and submitted to a heat treatment of $3\ K \cdot min^{-1}$ from room temperature to 773 K. Typically, a XANES spectrum was obtained every 10–15 K in a few seconds recording process. Notice that although the temporal resolution inherent to a dispersive XANES experiment is not absolutely necessary to follow the reduction process, it certainly gives a larger cleanness to the data, eliminating the average over the compositional (phase) change always present in conventional XANES data. This point may be of particular significance in the region of maximum variation of the reduction process.

The set of XANES spectra taken during the reduction treatment is analyzed using principal component factor analysis (PCA), details of which can be found in Refs. (8, 16). The PCA assumes that the absorbance in a set of spectra can be mathematically modeled as a linear sum of individual components, called factors, which correspond to each one of the copper species present in a sample, plus noise (20). Notice that this analysis does not intend to *decompose a specific copper species* in a linear combination of well-defined references, as erroneously assumed in Ref. (19). To determine the number of individual components, an F-test of the variance associated with factor k and the summed variance associated with the pool of noise factors is performed. A factor is accepted as a "pure" species (factor associated with signal and not noise) when the percentage of significance level of the F-test, %SL, is lower than a test level recommended by previous experience (5%) (8, 16, 17). The ratio between reduced eigenvalues, $R(r)$, and an empirical function, IND, defined by Malinowsky (18) will be also used in reaching this decision. Once the number of individual components is set, XANES spectra corresponding to individual copper species and their concentration profiles are generated by an orthogonal rotation (varimax rotation) which should align factors (as close as possible) along the unknown concentration profiles, followed by iterative transformation factor analysis (ITFA). ITFA starts with delta function representations of the concentration profiles located at temperatures predicted by the varimax rotation which are then subjected to refinement by iteration until the error in the resulting concentration profiles is lower than the statistical error extracted from the set of raw spectra (8, 16). XANES-based simulations of the hydrogen consumption produced by copper reduction were obtained by deriving the oxidized species (e.g., Cu^{2+} and Cu^+) concentration profiles throughout the reduction coordinate.

TEM experiments were carried out using a JEOL 2000FXII (0.31 nm point resolution) equipped with a LINK probe for EDS analysis. Microscopy samples were crushed in an agate mortar and suspended in cyclohexane. After ultrasonic dispersion, a droplet was deposited on a nickel grid supporting a perforated carbon film. Several portions of the sample were examined at low magnifications performing simultaneous EDS analysis. Electron difractograms, micrographs, and, when necessary, dark-field images were

recorded for selected areas of the sample with compositions previously characterized by EDS.

Conventional TPR experiments were performed using the same experimental conditions above described in a U-shaped quartz reactor. Effluents were monitored with a thermal conductivity detector connected to the exit of a Porapack Q column. Individual analyses were carried out at intervals of 2.5 min. Complementary solid state characterization was performed using X-ray diffraction (XRD) and UV-visible spectroscopy.

RESULTS

Figures 1A and 2A show representative XANES raw spectra of the series of approximately 25 taken during the reduction treatments of the 3% $Cu/Al_2O_3(OH)$ and 5% $Cu/Al_2O_3(H)$ samples, respectively. Simple visual inspection of these figures affords knowing that the 3% $Cu/Al_2O_3(OH)$ sample is reduced more smoothly and at higher temperatures than the other sample; however, as noted in the Introduction, the lack of information regarding the number of chemical species and their characteristic XANES spectra disables the extraction of additional information by, for example, fitting procedures. Clearly, the knowledge of the number of pure species is a first basic step towards the understanding of the reduction process. For both catalysts, Table 1 shows %SL values above the cutoff of 5% from factor 5 upwards; also from this factor the $R(r)$ approaches one. Finally, the minimum of the IND function also agrees in the election of four as the number of chemical species. The corresponding four XANES spectra are shown in Figs. 1B and 2B for the 3% $Cu/Al_2O_3(OH)$ and 5% $Cu/Al_2O_3(H)$ samples, respectively. Spectra of Cu^{2+} reference compounds, CuO and superficial and bulk $CuAl_2O_4$, are also included in these figures. The superficial copper aluminate reference corresponds to a low loading (1%) copper-on-alumina catalyst in which XPS detects only copper ions in octahedral positions of the aluminate phase (binding energy 934.2 eV) (21, 22).

TABLE 1

Principal Components Factor Analysis Results

Factor	Eigenvalue	%SL	$R(r)$	IND $\times 10^4$	Variance[a]
3% $Cu/Al_2O_3(OH)$					
1	323.611	0.00	150.37	4.473	99.390
2	1.94173	0.00	42.21	0.818	0.597
3	0.04105	0.00	23.84	0.229	0.012
4	0.00153	0.93	5.58	0.155	0.001
5	0.00024	14.32	1.67	0.159	
6	0.00012	20.71	2.10	0.175	
7	0.00005	38.09	0.99	0.301	
8	0.00004	39.53	0.88	0.427	
5% $Cu/Al_2O_3(H)$					
1	314.212	0.00	73.64	6.314	99.785
2	3.83883	0.00	190.45	0.630	0.207
3	0.01802	0.66	24.61	0.420	0.006
4	0.00647	0.00	28.51	0.132	0.002
5	0.00020	11.03	1.97	0.135	
6	0.00009	19.59	1.61	0.144	
7	0.00005	28.05	1.31	0.172	
8	0.00003	34.14	1.03	0.224	

[a] Variance is given in percentage. Values lower than 10^{-3} are not reported.

Both samples present in the TEM micrographs a dominant ill-crystallized phase of acicular appearance and a small fraction of large crystals (Fig. 3). Electron diffraction patterns recorded on these two areas are presented in Figs. 4A and 4B for the 3% $Cu/Al_2O_3(OH)$ sample while Fig. 4C shows the corresponding to an ill-crystallized portion of the 5% $Cu/Al_2O_3(H)$ specimen. On both samples, the ill-crystallized zones show rings ascribable to alumina and copper aluminate. No other copper phase is observed. In Fig. 4, diffraction patterns corresponding to two $[\bar{1}12]$ oriented Cu_2O large crystals (visible on the top of Fig. 3A) are also presented. In this case, it seems that the high vacuum conditions and/or the electron beam of the microscope induce the reduction of CuO crystals probably due to their thin section. Dark-field images of the $CuAl_2O_4$-like phase in contact with alumina of both samples were obtained and the corresponding particle size distributions measured, counting more than 750 particles presented in Fig. 5.

Finally, conventional TPR experiments are compared with XANES-based simulated ones in Figs. 6A and 6B. The reduction processes, expressed as hydrogen consumption, are depicted for each individual reducible Cu^{2+}/Cu^{+} phase, assuming formal stoichiometries (for instance, $CuO + H_2 \rightarrow Cu^0 + H_2O$). The linear sum of the contributions from individual copper species is given as a solid line.

DISCUSSION

The first significant difference between these two catalysts is the detection of a CuO-like species for 3% $Cu/Al_2O_3(OH)$, whereas only phases assignable to copper aluminates appear for 5% $Cu/Al_2O_3(H)$. Factor analysis identifies two types of copper aluminates. The first one corresponds to a superficial aluminate (called $CuAl_2O_4$-o; species 1 in Figs. 1B and 2B), similar, except in fine details of the local order/disorder denoted by a small energetic shift in the continuum resonance at $\approx$8997 eV, to a reference spectrum of low loading copper (1%) for both catalysts. The second one (species 2 in Fig. 2B), here called "bulk-like" or $CuAl_2O_4$-t/o which, due to the larger linewidth of the continuum resonance at $\approx$9000 eV (that contains contributions from octahedral and tetrahedral cations at $\approx$8997 and 9002 eV, respectively), resembles to a greater extent the local order around copper centers present in a highly crystalline $CuAl_2O_4$ phase spectrum

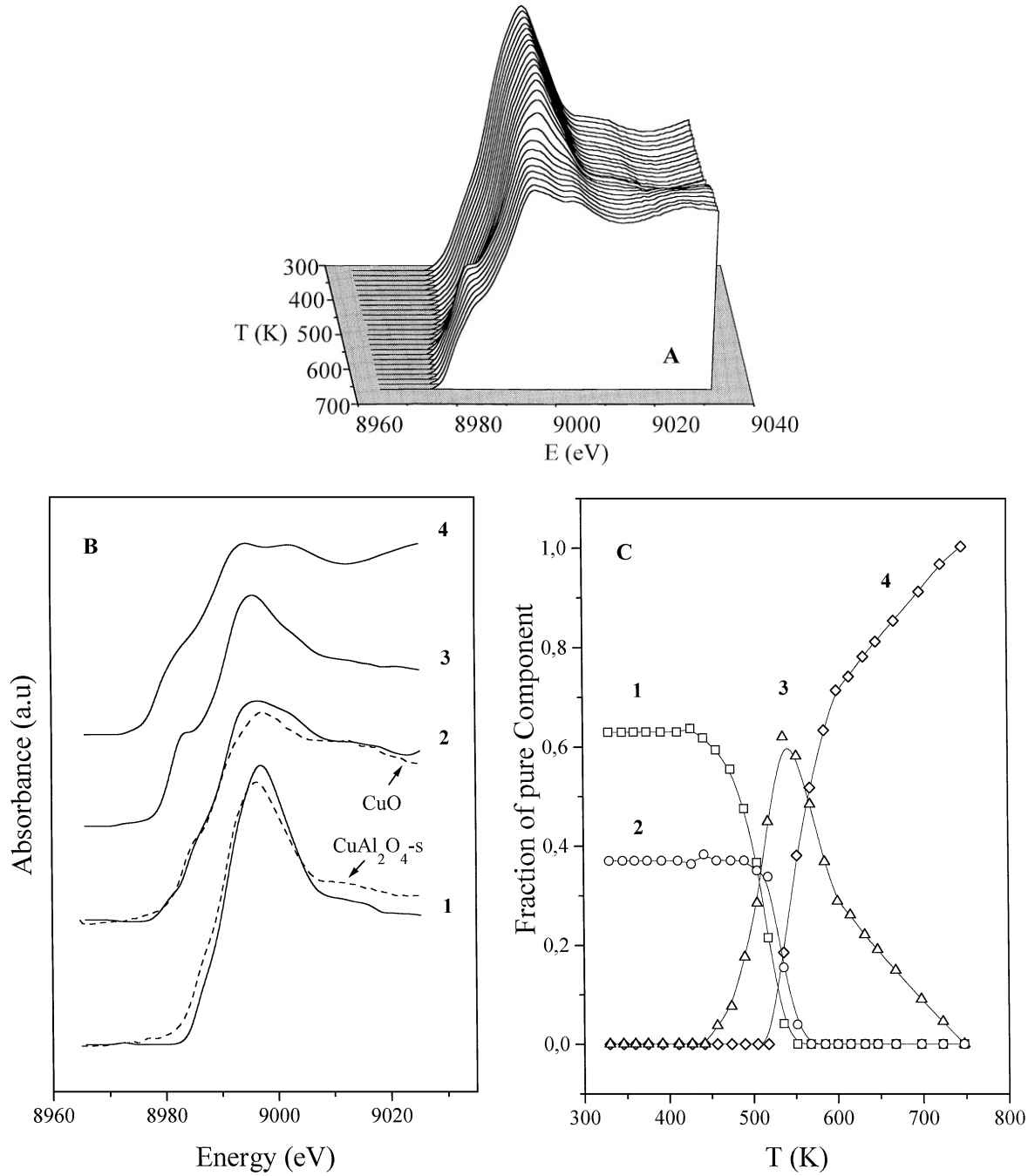

FIG. 1. XANES-TPR data for 3% $Cu/Al_2O_3(OH)$. **A**, Representative Cu K-edge XANES spectra. **B**, Predicted XANES spectra of individual copper species (solid lines) and reference compounds (dashed lines): 1, $CuAl_2O_4$-o phase; 2, CuO-like phase; 3, $CuAlO_2$ phase; 4, Cu^0 phase; $CuAl_2O_4$-s, superficial copper aluminate reference; CuO, copper oxide reference. **C**, Concentration profiles of the pure components along the reduction coordinate. Solid lines are only included as a guide for the eyes.

(corresponding to the dotted line in Fig. 2B). Notice that the $CuAl_2O_4$-t/o phase has a short or local order around copper cations (which is the physico-chemical property probed by XANES), similar to that of bulk $CuAl_2O_4$, but which does not have any other common similarity, especially that concerning long or three-dimensional order. The shape differences observed between reference surface/bulk copper aluminate XANES spectra are induced by the Cu^{2+} local symmetry; while the superficial phase has only copper in octahedral positions, the bulk phase contains Cu^{2+} in both octahedral (40%) and tetrahedral (60%) environments (21). Our $CuAl_2O_4$-o and $CuAl_2O_4$-t/o phases approach

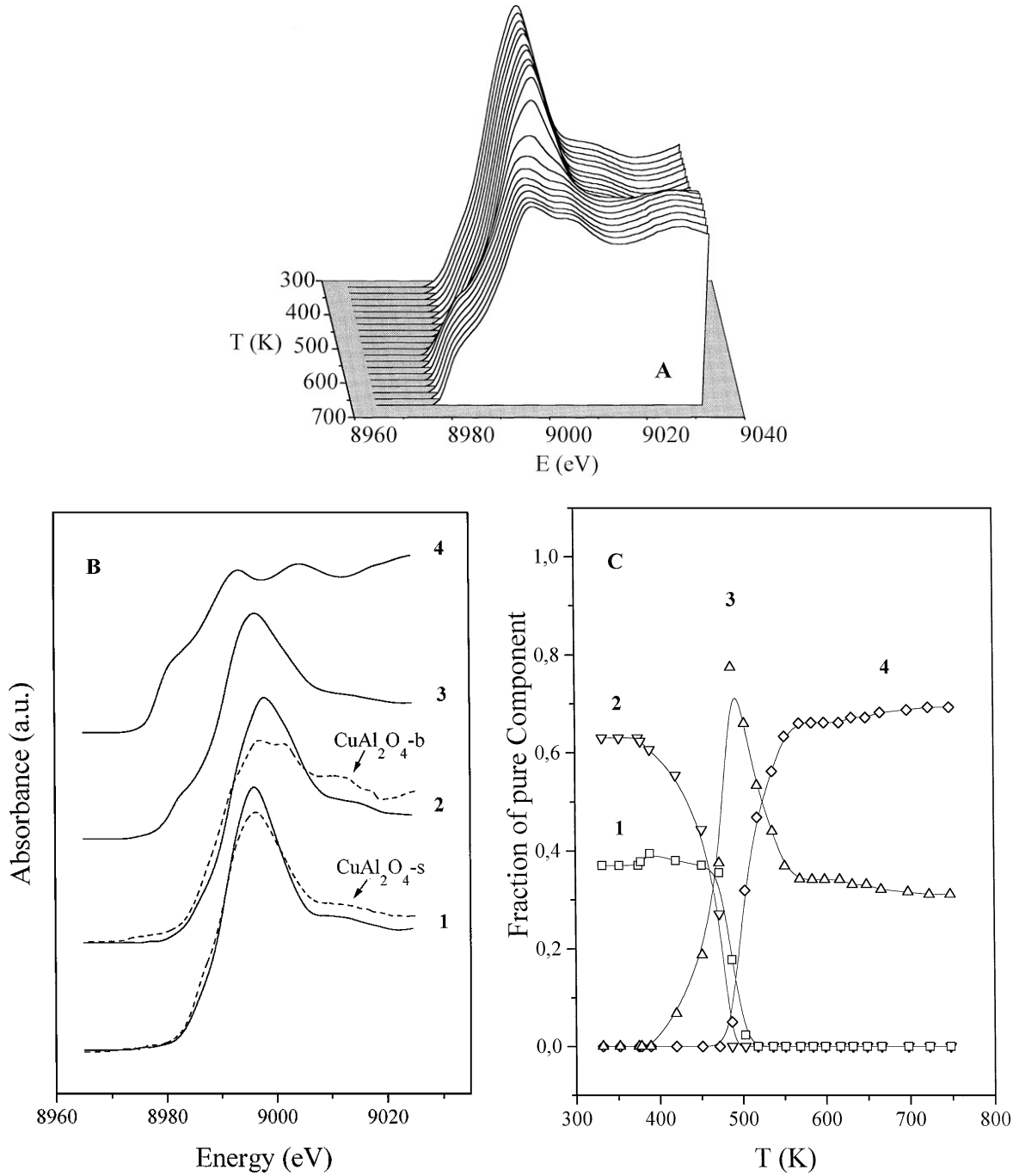

FIG. 2. XANES-TPR data for 5% Cu/Al_2O_3(H). **A**, Representative Cu K-edge XANES spectra. **B**, Predicted XANES spectra for individual copper species (solid lines) and reference compounds (dashed lines): 1, $CuAl_2O_4$-o phase; 2, $CuAl_2O_4$-t/o phase; 3, $CuAlO_2$ phase; 4, Cu^0 phase; $CuAl_2O_4$-s, superficial copper aluminate reference; $CuAl_2O_4$-b, bulk copper aluminate reference. **C**, Concentration profiles of the pure components along the reduction coordinate. Solid lines are only included as a guide for the eyes.

these situations, although we are not able to detail their exact copper distributions. As the percentage of copper loading used on both samples is lower than the formal one corresponding to monolayer coverage, i.e., to a surface aluminate phase, the appearance of bulk-like copper aluminate would be considered unlikely. However, using an acidic solution during the preparation procedure, part of the Al_2O_3 support is disolved and can react with Cu^{2+} ions to form an amorphous (not detectable by XRD) bulk-like copper aluminate after calcination. On the other hand,

FIG. 3. TEM images for the 3% $Cu/Al_2O_3(OH)$ (3a) and 5% $Cu/Al_2O_3(H)$ (3b) catalysts. In 3a an arrow locates a Cu_2O-like microcrystal (see text for details).

using a basic medium during the preparation stage, once the support surface reaches a certain coverage (dependent on preparation conditions) with copper, the additional quantity of Cu^{2+} interacts less strongly with the alumina and forms a dispersed CuO-like phase after calcination.

The TEM data support the initial, oxidized copper phase distribution obtained from the factorial analysis of the XANES data. The 3% $Cu/Al_2O_3(OH)$ sample shows weak rings ascribable to oxidized copper aluminate and an indication of the ease of the system to form copper oxide. In

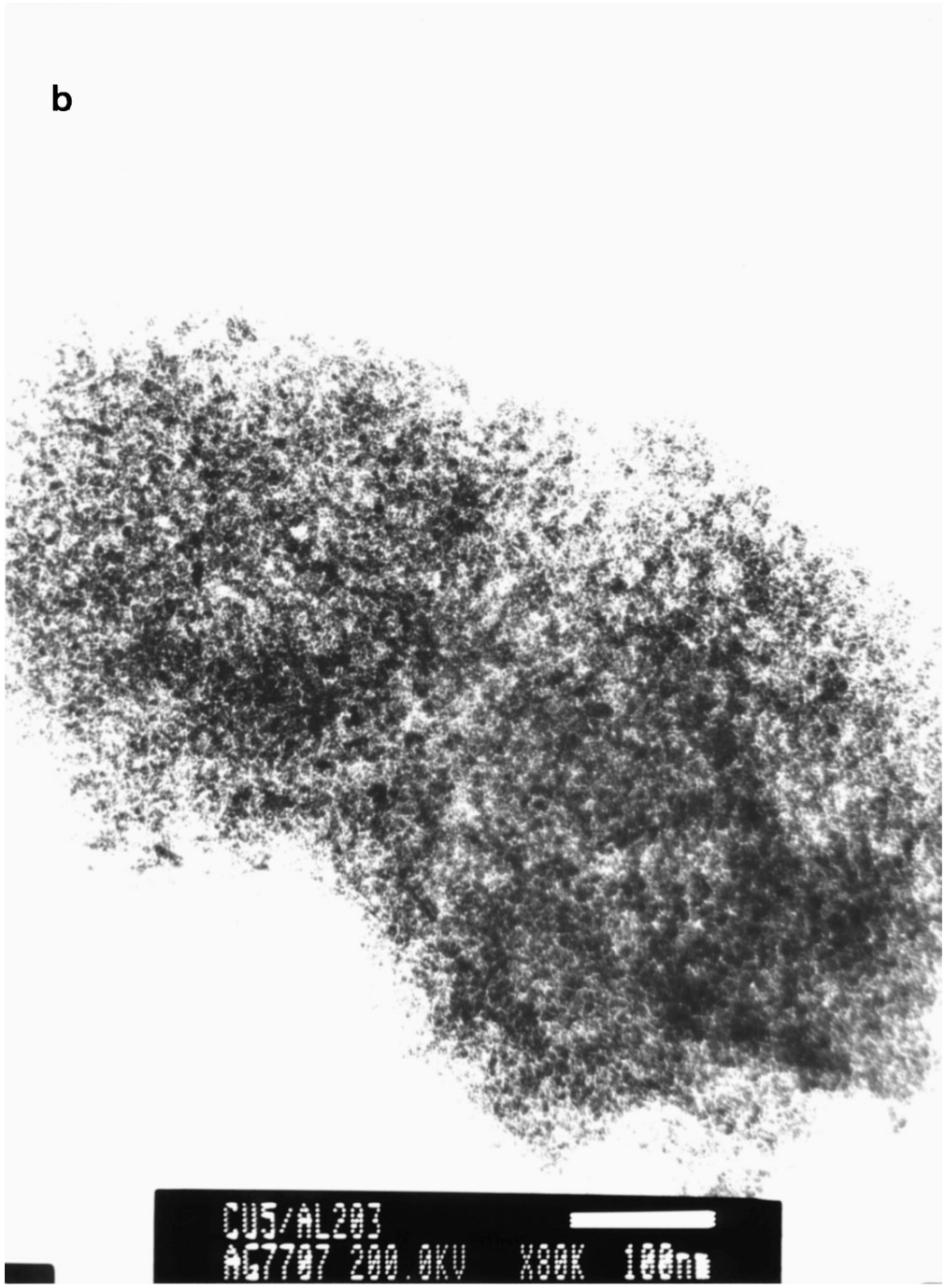

FIG. 3—*Continued*

contrast, the 5% Cu/Al_2O_3(H) catalyst, which is prepared in the usual way, impregnation, mainly contains copper aluminate in contact with alumina with no indication of the copper oxide phase presence, in complete agreement with a recent report (22).

In short, the XANES analysis (corroborated by TEM data) is able to show the profound implications of the preparation step in the nature of the active solid state phases present in a catalyst after calcination. Obviously, the catalytic consequences of the initial copper phase distribution are functions of the nature of the reaction being studied; for instance, for the catalytic reduction of nitrogen oxides highly dispersed (small) CuO-like aggregates correspond to the active sites (8), consequently basic solution preparations would be the optimum choice to obtain highly active systems.

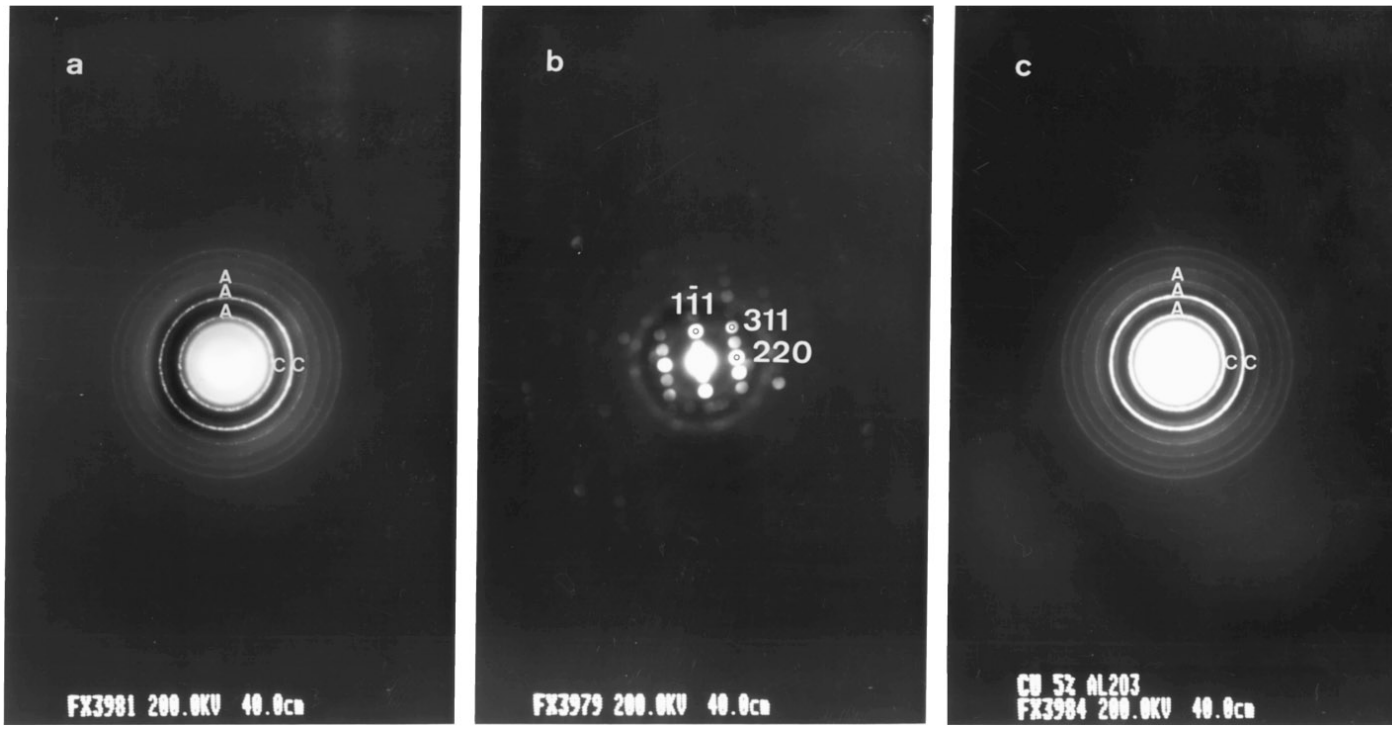

FIG. 4. Electron diffraction diagrams for two different zones of the 3% $Cu/Al_2O_3(OH)$ specimen (4a and 4b) and for one of the 5% $Cu/Al_2O_3(H)$ catalyst (4c). In Figs. 4a, c rings are assigned to: (A) alumina and (C) copper aluminate components. In 4b, the diffraction pattern of two [112] oriented Cu_2O crystals (shown in Fig. 3a) is assigned.

The evolution of these Cu^{2+} phases during the TPR experiment can be followed in Figs. 1C and 2C. For 3% $Cu/Al_2O_3(OH)$, the $CuAl_2O_4$ surface spinel reduction begins at a lower temperature than the CuO-like phase. The $CuAl_2O_4$-o phase is reduced in two steps, with intermediate formation of a $CuAlO_2$ surface spinel (species 3 in Figs. 1B and 2B), while CuO directly generates metallic copper (species 4 in Figs. 1B and 2B). The window of existence and the temperature of Cu^+ maximum concentration

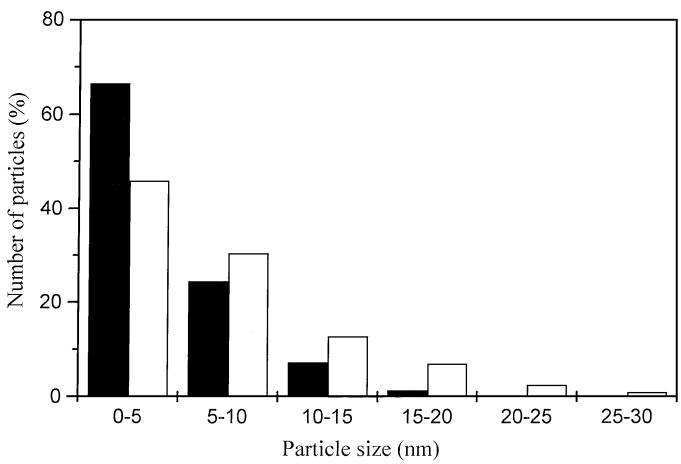

FIG. 5. Particle size histograms (from dark-field images) for the 3% $Cu/Al_2O_3(OH)$ (open bars) and 5% $Cu/Al_2O_3(H)$ (closed bars) catalyst.

are yielded by the analysis, both parameters being clearly affected by the catalyst preparation conditions. It must be noted that the presence of Cu^+ stabilized in an aluminate matrix has previously been detected by other physical techniques (XPS, DRS, ...) (23) and infrared spectroscopy of adsorbed CO (10), but no detailed information concerning the region of stability and chemical reactivity of this species was feasible to be reported. Note also that Cu^+ cations inserted in a CuO-like matrix, claimed to exist by several IR experiments using CO as a probe molecule (9, 10), must correspond to a minority state (of copper) even in a reasonable dispersed catalysts (i.e., high surface-to-bulk ratio phases) as no signal attributable to this species was observed. On the other hand, for the 5% $Cu/Al_2O_3(H)$ catalyst (Fig. 2C) we initially detect the reduction of the $CuAl_2O_4$-t/o phase and, only at higher temperatures, that of $CuAl_2O_4$-s. Both Cu^{2+} aluminates yield the same Cu^+ phase (copper in $CuAlO_2$ only occupies twofold linearly coordinated sites) on reduction.

Notable is the experimental temperature difference observed for the onset of the reduction process of the aluminate phases for both samples. Since the occupation of octahedral positions by copper in aluminate matrixes is thermodynamically favored (10), the chemical reactivity of Cu^{2+} ions in tetrahedral positions is expected to be higher and, therefore, the $CuAl_2O_4$-t/o phase should start its reduction at lower temperatures than the $CuAl_2O_4$-o one. Apart

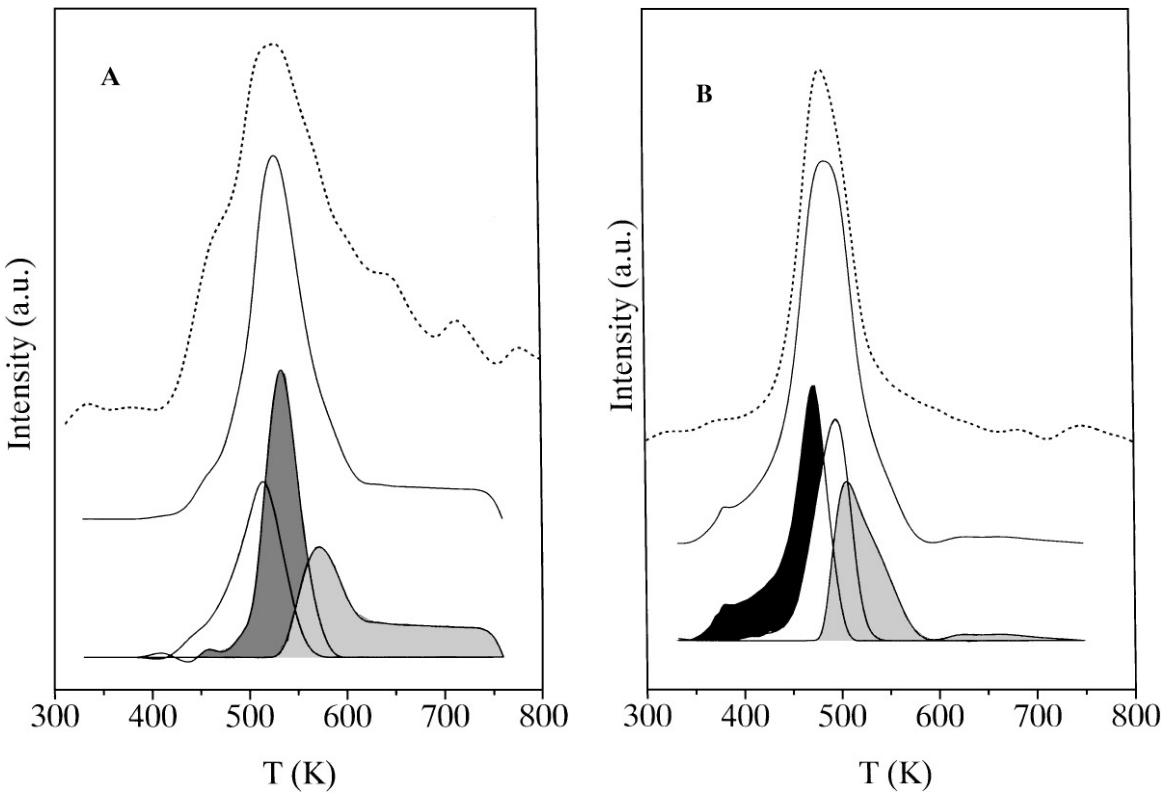

FIG. 6. XANES-based decomposition of the hydrogen consumption occurred during TPR experiments. **A**, 3% $Cu/Al_2O_3(OH)$. **B**, 5% $Cu/Al_2O_3(H)$. Black, $CuAl_2O_4$-o contribution; dark gray, CuO-like contribution; white, $CuAl_2O_4$-t/o contribution; light gray, $CuAlO_2$ contribution. Linear sum of the individual contributions is shown in full line. Conventional TPR data (dashed line) are included for comparison (see text for details).

from thermodynamical reasons, the phase reduction order of all copper phases present in both catalysts, that can be easily visualized in Fig. 6, may be interpreted in terms of two variables: particle size and surface characteristics (i.e., vacants/crystalline imperfections). The XRD failure in detecting any copper phase indicates that all of them have an average crystalline size smaller than 4 nm. Because both catalysts have a multiphase copper distribution, the typical use of characterization techniques as EXAFS to measure particle size will yield average values hardly interpretable. The dark-field images give, however, phase-selective information, although restricted to aluminate phases. Figure 5 shows that the corresponding size distribution is broader for the 3% $Cu/Al_2O_3(OH)$ specimen and has a pronounced tail extending up to 30 nm. To interpret this result, we must keep in mind that the 5% $Cu/Al_2O_3(H)$ catalyst distribution is dominated by the bulk-like copper aluminate while the 3% $Cu/Al_2O_3(OH)$ has only a contribution from the superficial one. Additionally, the superficial copper aluminate particle size is probably driven by that corresponding to the alumina support. Considering these arguments, we may conclude that the bulk-like aluminate has an average size smaller than the superficial one. On the other hand, the not-so-different particle size distribution of both catalysts (that can be rationalized by a smaller average particle size for the bulk-like aluminate) suggests that the differences observed in the reduction behavior of the superficial copper aluminate of both samples are primarily governed by the superficial characteristics of this phase. As hydrogen dissociation on oxides is a highly activated reaction (24), the existence of a different number and nature of surface oxygen vacancies that will generate electron-rich copper cations with a larger potential to initiate the dissociation of hydrogen may be the key factor in explaining the present results.

The 5% $Cu/Al_2O_3(H)$ sample shows an amount of Cu^+ after reduction at 773 K, a fact that may be explained considering that reduction of Cu^+ ions in the $CuAlO_2$ phase involves copper migration towards the external surface (9). Clearly, this process is restricted to the outermost regions of the aluminate particles, leaving a core with partially oxidized copper (Cu^+) at reduction temperatures below 773 K. In both systems, Cu^0 particles are formed at temperatures above 500 K. The better defined continuum resonances of the 5% $Cu/Al_2O_3(H)$ sample (see species 4 in Figs. 1C and 2C) indicates the large number of atoms (large particle size)

present in the zero-valent clusters of this catalyst with respect to 3% $Cu/Al_2O_3(OH)$ (18), despite the fact that the copper content of the zero-valent phases is the same in both catalysts because about 30% of the active metal is not reduced in the 5% $Cu/Al_2O_3(H)$ specimen at temperatures below 773 K. As the particle size of the majority oxidized phase is smaller in the last-mentioned catalyst, it may be considered that sintering effects play a major role in driving the differential behavior of both samples during the reduction process.

To highlight the new insights offered by this XANES study in the complex chemistry of the reduction process of copper on alumina catalysts, conventional TPR experiments are compared with XANES-based simulated ones in Figs. 6A and 6B. Although a quantitative match of both types of experiments cannot be achieved due to the important differences in the experimental setups and the neccessary simplifications made to estimate the hydrogen consumption from XANES results, the correspondence observed in both the range and maximum temperature of reduction reinforces our confidence in the goodness of the XANES analysis and results. It should be noted, however, that some shape differences for the 3% $Cu/Al_2O_3(OH)$ specimen are observed at the lower side of the TPR peak. This may be attributed to an overestimation of the CuO-like phase hydrogen consumption probably due to an unrealistic estimation of the reduction process stoichiometry originated by the presence of oxygen vacants (small particle size).

The huge difference in the reduction behavior of samples prepared in acid or basic conditions is again evidenced in the conventional TPR peak maxima and shapes, although information concerning existent phases and chemical behavior is strongly limited. The XANES-based decomposition gives, however, the key information which allows these differences to be properly interpreted. While the 3% $Cu/Al_2O_3(OH)$ sample TPR is dominated by the CuO contribution due to the step-like reduction of the aluminate, which spreads the corresponding hydrogen consumption over a large temperature range, for 5% $Cu/Al_2O_3(H)$ the absence of this CuO-like phase and the chemical similarity between the Cu^{2+} phases present (both aluminates) induces a strong overlap among the individual contributions and leads to an apparent "single" peak.

Another interesting feature visible in Figs. 6A and 6B is the considerable shift in temperature for reduction of the $CuAlO_2$ phase for the two samples. Again, this can be attributed to the combined effect of the different particle sizes and superficial characteristics (i.e., crystalline imperfections) of both samples, although the genesis of this phase (which is only present at the surface of the catalysts) makes the second point much more important. A large number of oxygen vacancies may exist in the Cu^+ aluminate of the 5% $Cu/Al_2O_3(H)$ catalyst as these Cu^+ cations seem to have a significantly larger 4sp electron occupation (less intense continuum resonance at ≈8983 eV). The catalytic effect of these vacancies in the hydrogen dissociation may thus explain the downward shift in the reduction temperature of the $CuAlO_2$ phase observed for the 5% $Cu/Al_2O_3(H)$ sample with respect to the 3% $Cu/Al_2O_3(OH)$ specimen.

CONCLUSIONS

Using this XANES/factor analysis methodology it has been demonstrated that basic solution preparations favor the presence of CuO-like phases in intimate contact with the support, while acid solution preparations tend to produce copper aluminate phases (if the calcination temperature is high enough). This has been confirmed by using TEM. The analysis gets, even in overlapping traces, the characteristic reduction temperatures of the copper phases, which seem to be strongly dependent on the superficial characteristics of the solids and (to a lesser extent) on the particle size of the initial, oxidized phases. Consequently, the same phase (e.g., $CuAl_2O_4$-o, or $CuAlO_2$) presents quite different maximum temperature of reduction depending on the preparation procedure of the catalyst. The analysis also reveals the two-step reduction mechanism of copper aluminates with appearance of a stable Cu^+ aluminate, the migration of Cu^+ ions towards the surface as a previous step for completion of the aluminate phase reductions, the (expected) direct copper oxide reduction to metallic copper, and, finally, the order of reactivity with H_2 for the two well-dispersed catalysts studied ($CuAl_2O_4$-t/o > $CuAl_2O_4$-o > CuO). All of this builds up the entire picture of the complex reduction process, in contrast with the partial view yielded by conventional methods.

ACKNOWLEDGMENTS

We thank the scientific staff of line ID-24 at the ESRF Synchrotron, Grenoble, for their help during XANES experiments and Mr. A. García for the TEM experiments. The critical reading of this manuscript by Dr. J. A. Anderson is gratefully appreciated. M.F.-G. acknowledges the Consejo Superior de Investigaciones Científicas (CSIC) for a Postdoctoral Contract. P.F.-A. thanks the Comunidad de Madrid for a scholarship grant. This work was partially supported by CICYT and DGICYT (Spain) under Projects MAT96-0859 and PB94-0077, respectively.

REFERENCES

1. Fierro, J. L. G., (Ed.), "Spectroscopic Characterization of Heterogeneous Catalysts," Studies in Surface Science and Catalysis, Vol. 57. Elsevier, Amsterdam, 1990.
2. Boudart, M., *Chem. Rev.* **95**, 661 (1995).
3. Bond, C. G., "Heterogeneous Catalysis: Principles and Applications," Clarendon Press, Oxford, 1987.
4. Somorjai, G. A., "Introduction to Surface Chemistry and Catalysis." Wiley, New York, 1994.
5. Hutchings, G. J., Desmartin-Chomel, A., Olier, R., and Volta, J.-C., *Nature* **368**, 41 (1994).
6. Smith, A. W., and Quets, J. M., *J. Catal.* **4**, 163 (1965).

7. Behara, R., *Appl. Catal.* **16**, 15 (1985).
8. Márquez-Alvarez, C., Rodríguez-Ramos, I., Guerrero-Ruiz, A., Haller, G. L., and Fernández-García, M., *J. Am. Chem. Soc.* **119**, 2905 (1997).
9. Tikhov, S. F., Sadykov, V. A., Kruyukova, G. N., Paukshtis, E. A., Pôpovskii, V. V., Starostina, T. G., Kharlamov, G. V., Anufrienko, V. F., Poluboyarov, V. F., Razdovarov, V. A., Bulgakov, N. N., and Kalinkin, A. V., *J. Catal.* **134**, 506 (1992).
10. Sepulveda, A., Márquez, C., Rodríguez-Ramos, I., Guerrero-Ruiz, A., and Fierro, J. L. G., *Surf. Interface Anal.* **20**, 1067 (1993).
11. Dow, H.-P., Wang, Y.-P., and Huang, T.-J., *J. Catal.* **160**, 155 (1996).
12. Rodríguez-Ramos, I., Guerrero-Ruiz, A., and Fierro, J. L. G., *Appl. Catal.* **72**, 119 (1991).
13. Niemantsverdricht, J. W., "Spectroscopy in Catalysis. An Introduction," VCH, Boca Raton, FL, 1996.
14. Shannon, I. J., Rey, F., Sankar, G., Thomas, J. M., Maschmeyer, Th., Waller, A. M., Palomares, A. E., Corma, A., Dent, J. A., and Greaves, G. N., *J. Chem. Soc. Faraday Trans.* **92**, 4331 (1996).
15. Hilbrig, F., Michel, C., and Haller, G. L., *J. Phys. Chem.* **96**, 9893 (1992).
16. Fernández-García, M., Márquez-Alvarez, C., and Haller, G. L., *J. Phys. Chem.* **99**, 12565 (1995).
17. Fernández-García, M., Anderson, J. A., and Haller, G. L., *J. Phys. Chem.* **100**, 16247 (1996); Fernández-García, M., Márquez-Alvarez, C., Rodríguez-Ramos, I., Guerrero-Ruiz, A., and Haller, G. L., *J. Phys. Chem.* **99**, 16380 (1995).
18. Greaves, G. N., Durham, P. J., Diakun, G., and Quinn, P., *Nature* **294**, 139 (1981).
19. Bazin, D. C., Sayers, D. A., and Rehr, J. J., *J. Phys. Chem. B* **101**, 11040 (1997).
20. Malinowsky, E. R., "Factor Analysis in Chemistry," Wiley, New York, 1991.
21. Friedman, R. M., Freeman, J. J., and Lytle, F. W., *J. Catal.* **55**, 10 (1978).
22. Fernández-García, M., Gómez-Rebollo, E., Guerrero-Ruiz, A., Conesa, J. C., and Soria, J., *J. Catal.* **172**, 146 (1997).
23. Strohmeier, B. R., Leiden, D. E., Field, R. S., and Hercules, D. M., *J. Catal.* **94**, 514 (1985).
24. Kiselev, V. F., and Krilov, O. V., "Adsorption and Catalysis on Transition Metals and Their Oxides," Springer Verlag, Hiedelberg, 1989.